

Symmetry Breaking of Self-Propelled Topological Defects in Thin-Film Active Chiral Nematics

Weiqliang Wang[✉], Haijie Ren[✉], and Rui Zhang^{✉*}

Department of Physics, The Hong Kong University of Science and Technology, Clear Water Bay, Kowloon, Hong Kong SAR



(Received 11 June 2023; revised 9 October 2023; accepted 28 November 2023; published 17 January 2024)

Active nematics represent a range of dense active matter systems which can engender spontaneous flows and self-propelled topological defects. Two-dimensional (2D) active nematic theory and simulation have been successful in explaining many quasi-2D experiments in which self-propelled $+1/2$ defects are observed to move along their symmetry axis. However, many active liquid crystals are essentially chiral nematic, but their twist mode becomes irrelevant under the 2D assumption. Here, we use theory and simulation to examine a three-dimensional active chiral nematic confined to a thin film, thus forming a quasi-2D system. We predict that the self-propelled $+1/2$ disclination in a curved thin film can break its mirror symmetry by moving circularly. Our prediction is confirmed by hydrodynamic simulations of thin spherical-shell and thin cylindrical-shell systems. In the spherical-shell confinement, the four emerged $+1/2$ disclinations exhibit rich dynamics as a function of activity and chirality. As such, we have proposed a new symmetry-breaking scenario in which self-propelled defects in quasi-2D active nematics can acquire an active angular velocity, greatly enriching their dynamics for finer control and emerging applications.

DOI: [10.1103/PhysRevLett.132.038301](https://doi.org/10.1103/PhysRevLett.132.038301)

Introduction.—Active matter encompasses a variety of far-from-equilibrium systems, in which individual constituents can persistently perform mechanical work, giving rise to collective behaviors that cannot occur in equilibrium systems [1–3]. As a paradigmatic active matter system, active liquid crystals (LCs) refer to LC systems that comprise autonomously moving units [4]. Examples include dense suspensions of cytoskeletal filaments and the corresponding motor proteins [5,6], dense bacteria suspensions [7], eukaryotic cells [8,9], or vibrating rods [10]. Active LCs can also be formed from doping active units into a passive LC, such as swimming bacteria dispersed in low-toxic lyotropic chromonic LCs [11] and microtubule-kinesin mixture dispersed in a colloidal LC [12]. Recent interests in active LCs are motivated by their potential applications in therapeutic delivery, photonic devices, and autonomous materials systems [4]. In active LCs, the collective motion of its active units can lead to the nucleation and self-propulsion of topological defects and spontaneous hydrodynamic flows. These emergent phenomena have been explained by theory and simulations [13–18]. Take two-dimensional (2D) active nematic as an example: Its cometlike $+1/2$ defect breaking head-tail symmetry tends to self-propel along its symmetry axis; whereas the trefoil-like $-1/2$ defect does not self-propel [15]. The moving direction of the $+1/2$ defect, whether from head to tail or from tail to head, can indicate the nature of the active stress as either contractile or extensile [15]. Recent research interest in active LCs has shifted from 2D to three-dimensional (3D) systems [12,19–22]. In the 3D

system, topological defects are more complex and dynamic than 2D point defects, making them more challenging to elucidate and control [23].

The success of 2D models in elucidating many active-nematic phenomena is based on the assumption that the underlying quasi-2D nematic confined to a thin cell or an oil-water interface is achiral [24]. However, many active LC units, such as actin filaments and microtubules, are chiral and can form a cholesteric (chiral nematic) phase at high concentrations [25]. In chiral nematics, neighboring molecules twist with respect to each other [26], resulting in periodic mesoscopic structures. In the existing theory and simulation efforts, the chirality of active nematics is often neglected. This achiral assumption is valid if the active LC system can be regarded as 2D, because the twist mode associated with chirality is intrinsically a 3D effect and becomes irrelevant in 2D.

In this work, we examine the validity of the above achiral assumption by studying a thin-film 3D active chiral nematic, in which the nematic directors in each plane of the film remain 2D and twist along the normal direction. We first study flat films and find that $+1/2$ defects also self-propel along their average orientation but at a slower speed compared to those in active achiral nematics. In a curved film, however, we theoretically predict that $+1/2$ defects can break their mirror symmetry by experiencing an additional transverse force, causing their circular motion. We further use hydrodynamic simulation to demonstrate this symmetry-breaking motion of defects by considering a thin spherical-shell active nematic, in which four $+1/2$

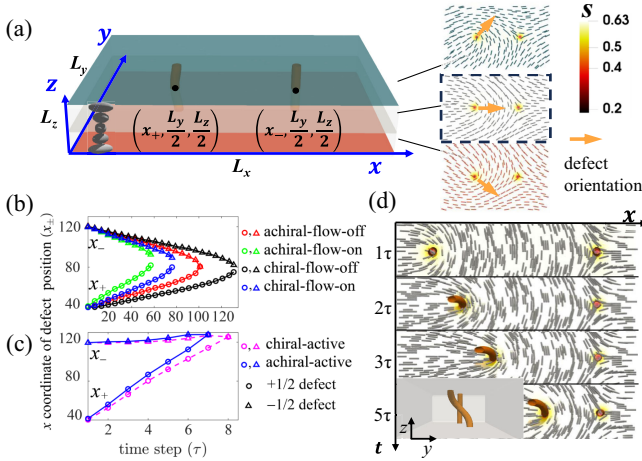


FIG. 1. Defect dynamics in a flat thin-film nematic. (a) Initially, a pair of $\pm 1/2$ disclinations (gray rods) are separated in the x direction. Gray grains illustrate the twisting of the director along the pitch direction. The director fields (short lines) in the top, middle, and bottom layers are shown on the right. The position and orientation of the winding in the midlayer (boxed) are used to represent the position and orientation of the disclination. (b) Defect positions as a function of time during annihilation for a passive nematic. (c) Defect positions as a function of time in an active nematic. (d) Kymograph of the defects in active chiral nematic. Inset: side view of the two defects. $\tau = 1000$ in simulation units.

defects move collectively. By varying the active stress (activity) and chirality parameter, we uncover a rich defect dynamics diagram, in which the defects move circularly in closed trajectories represented by triangles, squares, or other polygons. Consistent with our theory, these $+1/2$ defects exhibit counterclockwise (clockwise) rotation in right- (left-)handed chiral nematics. Such chiral motion of $+1/2$ defects is also found in thin cylindrical-shell active nematic systems, further confirming our prediction.

Results.—We first examine defect dynamics in a flat thin film using a well-developed hybrid lattice Boltzmann method [13,27–29] (see Supplemental Material, Sec. I [30]). Specifically, we prepare a pair of $\pm 1/2$ disclinations in a thin simulation box, which is periodic in both the x and y directions but confined by two narrowly spaced z walls, which impose a degenerate planar anchoring to a right-handed chiral nematic with the pitch axis pointing along the z direction [Fig. 1(a)]. We choose the ratio of pitch to box thickness to be $p/L_z = 6$ to approximate a thin film. Because the director \mathbf{n} twists along the z direction, the winding of the disclinations also rotates from the bottom to the top layer by $2\pi L_z/p = \pi/3$ [Fig. 1(a)]. Therefore, the system can be regarded as an ensemble of many 2D nematic layers, each of which corresponds to a different relative orientation of two point defects [Fig. 1(a)] [60,61]. In this thin-film system, there is a slight out-of-plane component for \mathbf{n} in bend-dominated regions near defects (see Supplemental Material, Fig. S1 [30]). By analyzing the

Frank elastic energy, we find that the nonzero n_z can help release the bend energy and is, thus, favored by the system (see Supplemental Material, Sec. II [30]).

We next analyze defect dynamics in the above system [Fig. 1(a)]. Since the $+1/2$ defect initially points toward the $-1/2$ defect, the pair will gradually approach each other and eventually annihilate under the combined influence of extensile active stress and elastic attractive force. By tracking the positions and orientations of the windings of the two defects on the midlayer $z = L_z/2$, we find that their speeds are always slower in chiral nematic than in achiral nematic [Figs. 1(b) and 1(c)]. The out-of-plane component of the director is responsible for the weakened elastic attractive force between the two defects in chiral nematics (see Supplemental Material, Fig. S1 [30]). The variation of the defect winding is responsible for the weakened hydrodynamic flow and active force that help accelerate the $+1/2$ defect. In the above system, the $+1/2$ defect remains moving straight along its orientation on the midlayer, showing no angular velocity.

We proceed to consider active defect dynamics in a curved thin film. This is motivated by the fact that the active force for a 2D active nematic is a function of surface curvature. To demonstrate, we consider an isolated $+1/2$ defect located at the north pole of a spherical surface of radius r . Similar to planar surfaces, we can write out the director field near the core as $\mathbf{n} = [\cos(\phi/2)]\hat{\theta} + [\sin(\phi/2)]\hat{\phi}$ with θ and ϕ being the polar and azimuthal angle, respectively. By calculating the local active force per area $\nabla \cdot (\mathbf{nn})$, we find it scales as $1/r$ (see Supplemental Material, Sec. III [30]). Therefore, the effective active force F acting on the defect scales as $F \sim \int dS \nabla \cdot (\mathbf{nn}) \sim \int d\Omega r^2 \nabla \cdot (\mathbf{nn}) \propto r$ (see Supplemental Material, Sec. III [30]). For a spherical shell, the active force acting on the winding of a $+1/2$ disclination is stronger near the outer surface than near the inner surface. For a right-handed chiral nematic, we thus expect that the $+1/2$ defect should tend to turn left (rotate counterclockwise) due to the net force along the orthogonal direction. A similar mechanism is found in active solids [63,64] (see Supplemental Material, Sec. III and Fig. S3 [30]). The same scaling of active force is also present in thin cylindrical shells (see Supplemental Material, Sec. III [30]).

To test the above theoretical predictions, we perform hydrodynamic simulations of an active chiral nematic confined to a concentric spherical shell with no slip and degenerate planar anchoring on both confining surfaces [Fig. 2(a)]. To approximate a thin film, the pitch to shell-gap ratio is chosen to be $p/\Delta R \equiv p/(R_2 - R_1) \in [13, 251] \gg 1$ ($q_0 \in [0.005, 0.098]$), at which the ground state of the system forms a “baseball-like” (tetrahedral) structure [65], with four $+1/2$ disclinations residing on the four vertices of a tetrahedron [62,66]. This ground state is similar to that of an achiral nematic in the same confinement, except that in the chiral system the disclination

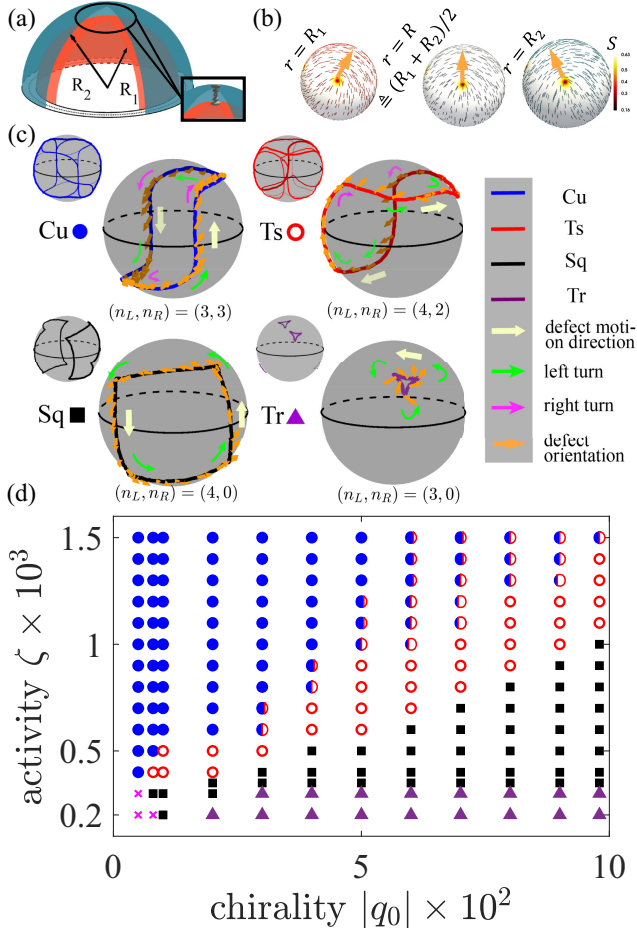


FIG. 2. Defect dynamics in a thin spherical-shell active chiral nematic. (a) A schematic of the spherical shell with inner radius R_1 and outer radius R_2 . (b) From left to right: director field on the inner, middle, and outer layer. (c) Defect trajectories for Cu, Ts, Sq, and Tr mode. Sharp turns are marked by green and magenta arrows. (d) Defect dynamics diagram. Markers correspond to the defect modes in (c). Magenta cross marks the static (St) mode in which the four $+1/2$ defects are in the tetrahedron configuration [62]. Partially filled circles represent a mixed Cu-Ts mode (Movies S5–S7; see Supplemental Material [30]).

winding rotates along the surface normal direction [66] [Fig. 2(b)]. In a relevant experiment involving microtubule-kinesin mixtures on a lipid vesicle surface, it was observed that four emerged defects move collectively in a periodic fashion [67]. This phenomenon was reproduced by a hydrodynamic simulation of a thin-shell active nematic, in which the four defects were found moving along a deformed cube on the sphere, thereby oscillating between the tetrahedral state and an excited planar state [29]. Here, we adopt the same model but include an additional chiral term in the elastic energy (see Supplemental Material, Sec. I [30]). We thereafter find rich defect dynamics as a function of activity ζ and chirality $q_0 \equiv 2\pi/p$. Specifically, we observe five distinct defect dynamics modes, namely “triangle” (Tr), “square” (Sq), “transition” (Ts), “cube”

(Cu), and “static” (St) mode using different parameter sets [Figs. 2(c) and 2(d)].

We next elaborate on these defect modes. For relatively low chirality ($0 < q_0 < 0.02$), there is a threshold activity below which the active stress is too weak to drive the system out of the tetrahedral structure; the system is, therefore, in the stationary (St) mode with the four defects remaining static. This threshold activity decreases as chirality increases [Fig. 2(d)]. When the chirality is sufficiently high ($q_0 \geq 0.02$), the system enters the triangle (Tr) mode, where the defects move in a closed triangle-like trajectory in the vicinity of their equilibrium positions [Fig. 2(c) and Supplemental Material, Movie S1 [30]]. For the right-handed chiral nematic considered here, the defects make left turns at the three corners of the trajectory, while their orientations are continuously rotating counterclockwise [Fig. 2(d)]. We use $(n_L, n_R) = (3, 0)$ to denote the three sharp left turns and no sharp right turns for the defect making one revolution in the Tr mode.

If the activity ζ is increased from the Tr mode, the system will enter the square (Sq) mode, in which the four defects group into two pairs, with each pair circulating on a closed square-like trajectory [Fig. 2(c) and Supplemental Material, Movie S2 [30]]. Similar chiral motion of defects can also be observed in active achiral nematics, in which mirror symmetry is broken locally and both handed motions are possible (see Supplemental Material, Sec. IX [30]). Similar to the Tr mode, each defect in the Sq mode continuously rotates counterclockwise while making four sharp left turns in one revolution [Fig. 2(c)]. Thus, $(n_L, n_R) = (4, 0)$. In this mode, the defects oscillate between the tetrahedral and planar structure, unlike the Tr mode, in which the system remains in the neighborhood of the tetrahedral structure (see Supplemental Material, Fig. S4 [30]).

When ζ is sufficiently high but q_0 is relatively low, the system is in the cubic (Cu) mode, which appears similar to the defect mode in the thin-shell active achiral nematic [29] [Fig. 2(c) and Supplemental Material, Movie S3 [30]]. Each defect trajectory can be regarded as a 3D hexagon, with its six sides following six edges of a cube [Fig. 2(c)], on which the defect makes three left turns and three right turns, i.e., $(n_L, n_R) = (3, 3)$, indicating that the defect has no chirality. Indeed, their orientational angular velocity ω is found to fluctuate about a zero mean (see Supplemental Material, Sec. IV [30] and Fig. S5).

When ζ is intermediate between the Cu and Sq modes, a transition (Ts) mode occurs, in which defect trajectories do not overlap [Fig. 2(c) and Supplemental Material, Movie S4 [30]]. The individual defect trajectory can be regarded as a bent rectangle [Fig. 2(c)], on which the defect makes four left turns and two right turns [$(n_L, n_R) = (4, 2)$]. Interestingly, near the Cu-Ts mode boundary on the diagram, defects can alternatively switch between these two modes, leading to a rich spectrum of defect dynamics [Fig. 2(d) and Supplemental Material, Movies S5–S7 [30]].

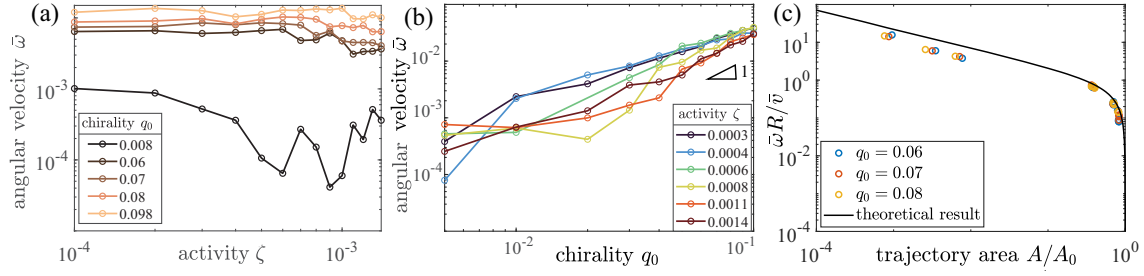


FIG. 3. Orientational angular velocity of defects and their trajectory areas on a sphere. (a) Mean angular velocity $\bar{\omega}$ as a function of ζ . (b) Mean angular velocity $\bar{\omega}$ as a function of q_0 . (c) Reduced mean angular velocity $\bar{\omega}R/\bar{v}$ against its trajectory area A scaled by hemispherical surface area $A_0 = 2\pi R^2$.

We further measure the angular velocities $\bar{\omega}$ of defects and find that they are invariant at low activity levels at fixed q_0 [Fig. 3(a) and Supplemental Material, Fig. S4 [30]]. Moreover, $\bar{\omega}$ scales linearly with q_0 , consistent with our theory, as more chiral system yields less aligned active force on the disclination windings [Fig. 3(b), Supplemental Material, Sec. III, and Fig. S6 [30]].

The above four different types of defect trajectories, namely, triangle, square, bent rectangle, and bent hexagon, are homeomorphic. However, they represent different levels of defect chirality. As q_0/ζ decreases, these modes (Tr, Sq, Ts, and Cu) appear in order, with the ratio $n_R/n_L = 0, 0, 1/2, 1$ increasing monotonically [Fig. 2(d)]. The sharp left turns of the defects can be understood by the interplay between their linear motion and rotation, as defects move approximately along its orientation while gradually rotating their orientations (see Supplemental Material, Sec. V [30]). There is also an interesting connection between defect chirality and the geometry of their trajectories. For an ideal chiral defect moving at a constant linear velocity v and constant angular velocity ω on a sphere of radius R , the surface area enclosed by its trajectory, or “trajectory area” in short, A , can be calculated via $(\omega R/v) = [(A_0 - A)/\sqrt{(2A_0 - A)A}]$ with $A_0 \equiv 2\pi R^2$ (see Supplemental Material, Sec. VI [30]). In our

simulation, $\bar{\omega}/\bar{v}$ follows the above theoretical relation. The deviation is due to the temporal variation of ω/v of the defects (see Supplemental Material, Fig. S5 [30]).

Our prediction of defect chirality also works for contractile systems. By setting $\zeta < 0$ in the above spherical-shell system, simulation finds that the defects can self-propel (see Supplemental Material, Sec. VII and Movie S8 [30]), in contrast to contractile active achiral nematics, in which defects are stationary [29].

To further demonstrate defect chirality in curved thin films, we examine an active chiral nematic confined to a thin concentric cylindrical shell [Fig. 4(a)]. The ground state of the chiral nematic in this confinement is a defect-free, double-twist cylinder structure, with its director twists along all radial directions (see Supplemental Material, Sec. VIII and Fig. S8 [30]). If one follows the director field on the midlayer of radius R , it leads to a left-handed helix with a pitch $p_d = 2\pi R \cot \theta$, where θ is the tilt angle of the director from the axial direction [Fig. 4(b)]. For an achirally moving point with the same orientation as the $+1/2$ defect, we expect that its trajectory is a right-handed helix with a pitch $p = 2\pi R \tan \theta$. However, our simulation gives rise to a defect trajectory with a longer pitch, indicating that the defect tends to rotate counterclockwise [Fig. 4(c) and Supplemental Material, Sec. VII, Fig. S9, and Movies S9 and S10 [30]]. We further find that the pitch increases as ζ decreases or q_0 increases (see Supplemental Material, Fig. S10 [30]), consistent with our expectations (see Supplemental Material, Sec. III [30]).

Discussion.—Active chiral nematics have been studied in terms of instability patterns and 3D defect dynamics [68–71]. However, quasi-2D active chiral nematics have not been explored. The chirality considered here is different from many existing works in which a self-spinning tendency of the active units results in a chiral stress [71,72]. We find that $+1/2$ defects in flat thin-film active chiral nematics exhibit no chirality except move slower. In curved thin films, however, $+1/2$ defects break their mirror symmetry by experiencing a net transverse force. Our hydrodynamic simulation confirms this prediction by showing that, in both spherical and cylindrical thin shells, $+1/2$ defects tend to self-propel in an off-axis direction.

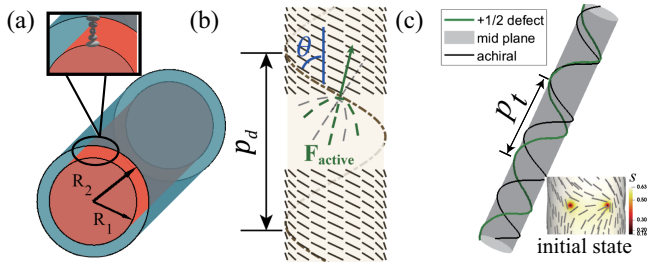


FIG. 4. Defect dynamics of a thin cylindrical-shell active chiral nematic. (a) A schematic of the cylindrical shell with inner radius R_1 and outer radius R_2 . (b) The director field on the midlayer. (c) $+1/2$ defect trajectory on the midlayer at $q_0 = 0.08$ and $\zeta = 0.004$; inset: initial defect configuration with color denoting S . The black curve represents the trajectory of an achirally moving point.

We also uncover rich defect dynamics in a thin spherical shell, which can be explained by the interplay of the linear motion and rotation of the defects.

In conclusion, our work presents a new symmetry-breaking scenario in quasi-2D active nematics in which defects can actively rotate. This additional degree of freedom can facilitate defect-based applications, such as dynamic self-assembly, material transport, and logic operations [73]. Active chiral nematic in a film of nonuniform curvature can be an interesting direction for future studies [74–77].

The work is supported by the Hong Kong Research Grants Council via Grant No. 26302320.

* ruizhang@ust.hk

- [1] R. Aditi Simha and S. Ramaswamy, *Phys. Rev. Lett.* **89**, 058101 (2002).
- [2] M. C. Marchetti, J. F. Joanny, S. Ramaswamy, T. B. Liverpool, J. Prost, M. Rao, and R. A. Simha, *Rev. Mod. Phys.* **85**, 1143 (2013).
- [3] D. Needleman and Z. Dogic, *Nat. Rev. Mater.* **2**, 1 (2017).
- [4] R. Zhang, A. Mozaffari, and J. J. de Pablo, *Nat. Rev. Mater.* **6**, 437 (2021).
- [5] T. Sanchez, D. T. N. Chen, S. J. DeCamp, M. Heymann, and Z. Dogic, *Nature (London)* **491**, 431 (2012).
- [6] N. Kumar, R. Zhang, J. J. de Pablo, and M. L. Gardel, *Sci. Adv.* **4**, eaat7779 (2018).
- [7] H. Li, X.-q. Shi, M. Huang, X. Chen, M. Xiao, C. Liu, H. Chaté, and H. Zhang, *Proc. Natl. Acad. Sci. U.S.A.* **116**, 777 (2019).
- [8] T. B. Saw, A. Doostmohammadi, V. Nier, L. Kocgozlu, S. Thampi, Y. Toyama, P. Marcq, C. T. Lim, J. M. Yeomans, and B. Ladoux, *Nature (London)* **544**, 212 (2017).
- [9] K. Kawaguchi, R. Kageyama, and M. Sano, *Nature (London)* **545**, 327 (2017).
- [10] V. Narayan, S. Ramaswamy, and N. Menon, *Science* **317**, 105 (2007).
- [11] S. Zhou, A. Sokolov, O. D. Lavrentovich, and I. S. Aranson, *Proc. Natl. Acad. Sci. U.S.A.* **111**, 1265 (2014).
- [12] G. Duclos, R. Adkins, D. Banerjee, M. S. Peterson, M. Varghese, I. Kolvin, A. Baskaran, R. A. Pelcovits, T. R. Powers, A. Baskaran *et al.*, *Science* **367**, 1120 (2020).
- [13] D. Marenduzzo, E. Orlandini, and J. M. Yeomans, *Phys. Rev. Lett.* **98**, 118102 (2007).
- [14] S. P. Thampi, R. Golestanian, and J. M. Yeomans, *Phys. Rev. Lett.* **111**, 118101 (2013).
- [15] L. Giomi, M. J. Bowick, P. Mishra, R. Sknepnek, and M. Cristina Marchetti, *Phil. Trans. R. Soc. A* **372**, 20130365 (2014).
- [16] A. Doostmohammadi, J. Ignés-Mullol, J. M. Yeomans, and F. Sagués, *Nat. Commun.* **9**, 3246 (2018).
- [17] R. C. Coelho, N. A. Araújo, and M. M. T. da Gama, *Soft Matter* **18**, 7642 (2022).
- [18] X.-q. Shi and Y.-q. Ma, *Nat. Commun.* **4**, 3013 (2013).
- [19] J. Binysh, Ž. Kos, S. Čopar, M. Ravnik, and G. P. Alexander, *Phys. Rev. Lett.* **124**, 088001 (2020).
- [20] S. Chandragiri, A. Doostmohammadi, J. M. Yeomans, and S. P. Thampi, *Phys. Rev. Lett.* **125**, 148002 (2020).
- [21] J. Binysh, J. Pollard, and G. P. Alexander, *Phys. Rev. Lett.* **125**, 047801 (2020).
- [22] M. R. Nejad and J. M. Yeomans, *Phys. Rev. Lett.* **128**, 048001 (2022).
- [23] T. N. Shendruk, K. Thijssen, J. M. Yeomans, and A. Doostmohammadi, *Phys. Rev. E* **98**, 010601(R) (2018).
- [24] M. Nestler and A. Voigt, *Commun. Comput. Phys.* **31**, 947 (2022).
- [25] L. N. Carenza, G. Gonnella, D. Marenduzzo, and G. Negro, *Proc. Natl. Acad. Sci. U.S.A.* **116**, 22065 (2019).
- [26] P. G. de Gennes and J. Prost, *The Physics of Liquid Crystals* (Oxford University Press, Oxford, 1995).
- [27] C. Denniston, D. Marenduzzo, E. Orlandini, and J. Yeomans, *Phil. Trans. R. Soc. A* **362**, 1745 (2004).
- [28] R. Zhang, T. Roberts, I. S. Aranson, and J. J. de Pablo, *J. Chem. Phys.* **144**, 084905 (2016).
- [29] R. Zhang, Y. Zhou, M. Rahimi, and J. J. de Pablo, *Nat. Commun.* **7**, 13483 (2016).
- [30] See Supplemental Material at <http://link.aps.org/supplemental/10.1103/PhysRevLett.132.038301> for the theoretical calculation, simulation method, and additional information in detail, which includes Refs. [31–59].
- [31] A. N. Beris, B. J. Edwards *et al.*, *Thermodynamics of Flowing Systems: With Internal Microstructure* (Oxford University Press, New York, 1994), Vol. 36.
- [32] C. Denniston, E. Orlandini, and J. M. Yeomans, *Phys. Rev. E* **63**, 056702 (2001).
- [33] M. Ravnik and S. Žumer, *Liq. Cryst.* **36**, 1201 (2009).
- [34] J.-B. Fournier and P. Galatola, *Europhys. Lett.* **72**, 403 (2005).
- [35] V. M. Batista, M. L. Blow, and M. M. T. da Gama, *Soft Matter* **11**, 4674 (2015).
- [36] J.-i. Fukuda, H. Yokoyama, M. Yoneya, and H. Stark, *Mol. Cryst. Liq. Cryst.* **435**, 63 (2005).
- [37] Y. Hatwalne, S. Ramaswamy, M. Rao, and R. A. Simha, *Phys. Rev. Lett.* **92**, 118101 (2004).
- [38] D. Marenduzzo, E. Orlandini, M. E. Cates, and J. M. Yeomans, *Phys. Rev. E* **76**, 031921 (2007).
- [39] Z. Guo and C. Shu, *Lattice Boltzmann Method and Its Application in Engineering* (World Scientific, Singapore, 2013), Vol. 3.
- [40] M. Kleman and O. D. Lavrentovich, *Soft Matter Physics: An Introduction* (Springer, New York, 2003).
- [41] J. L. Ericksen, *Mol. Cryst. Liq. Cryst.* **7**, 153 (1969).
- [42] F. M. Leslie, *Q. J. Mech. Appl. Math.* **19**, 357 (1966).
- [43] O. Parodi, *J. Phys.* **31**, 581 (1970).
- [44] W. Wang and R. Zhang, *Crystals* **11**, 1071 (2021).
- [45] S. Shankar, S. Ramaswamy, M. C. Marchetti, and M. J. Bowick, *Phys. Rev. Lett.* **121**, 108002 (2018).
- [46] S. Shankar and M. C. Marchetti, *Phys. Rev. X* **9**, 041047 (2019).
- [47] D. J. G. Pearce, J. Nambisan, P. W. Ellis, A. Fernandez-Nieves, and L. Giomi, *Phys. Rev. Lett.* **127**, 197801 (2021).
- [48] J. Plebanski and A. Krasinski, *An Introduction to General Relativity and Cosmology* (Cambridge University Press, Cambridge, England, 2006).
- [49] A. Javadi, J. Eun, and J. Jeong, *Soft Matter* **14**, 9005 (2018).

- [50] J. Eun, S.-J. Kim, and J. Jeong, *Phys. Rev. E* **100**, 012702 (2019).
- [51] A. T. Brown, *Soft Matter* **16**, 4682 (2020).
- [52] Y.-H. Zhang, M. Deserno, Z.-C. Tu *et al.*, *Phys. Rev. E* **102**, 012607 (2020).
- [53] D. Khoromskaia and G. P. Alexander, *New J. Phys.* **19**, 103043 (2017).
- [54] S. Henkes, M. C. Marchetti, and R. Sknepnek, *Phys. Rev. E* **97**, 042605 (2018).
- [55] F. Alaimo, C. Köhler, and A. Voigt, *Sci. Rep.* **7**, 5211 (2017).
- [56] P. Guillamat, Ž. Kos, J. Hardoüin, J. Ignés-Mullol, M. Ravnik, and F. Sagués, *Sci. Adv.* **4**, eaao1470 (2018).
- [57] R. C. Coelho, N. A. Araújo, and M. M. T. da Gama, *Soft Matter* **15**, 6819 (2019).
- [58] F. Caballero, Z. You, and M. C. Marchetti, *Soft Matter* **19**, 7828 (2023).
- [59] C. D. Schimming, C. J. O. Reichhardt, and C. Reichhardt, *Phys. Rev. Lett.* **132**, 018301 (2024).
- [60] A. J. Vromans and L. Giomi, *Soft Matter* **12**, 6490 (2016).
- [61] X. Tang and J. V. Selinger, *Soft Matter* **13**, 5481 (2017).
- [62] D. Seč, T. Lopez-Leon, M. Nobili, C. Blanc, A. Fernandez-Nieves, M. Ravnik, and S. Žumer, *Phys. Rev. E* **86**, 020705(R) (2012).
- [63] E. Ferrante, A. E. Turgut, M. Dorigo, and C. Huepe, *Phys. Rev. Lett.* **111**, 268302 (2013).
- [64] H. Xu, Y. Huang, R. Zhang, and Y. Wu, *Nat. Phys.* **19**, 46 (2023).
- [65] D. R. Nelson, *Nano Lett.* **2**, 1125 (2002).
- [66] Y. Zhou, A. Guo, R. Zhang, J. C. Armas-Perez, J. A. Martínez-González, M. Rahimi, M. Sadati, and J. J. de Pablo, *Soft Matter* **12**, 8983 (2016).
- [67] F. C. Keber, E. Loiseau, T. Sanchez, S. J. DeCamp, L. Giomi, M. J. Bowick, M. C. Marchetti, Z. Dogic, and A. R. Bausch, *Science* **345**, 1135 (2014).
- [68] C. A. Whitfield, T. C. Adhyapak, A. Tiribocchi, G. P. Alexander, D. Marenduzzo, and S. Ramaswamy, *Eur. Phys. J. E* **40**, 50 (2017).
- [69] L. Metselaar, A. Doostmohammadi, and J. M. Yeomans, *J. Chem. Phys.* **150**, 064909 (2019).
- [70] L. N. Carenza, G. Gonnella, D. Marenduzzo, and G. Negro, *Proc. Natl. Acad. Sci. U.S.A.* **116**, 22065 (2019).
- [71] S. J. Kole, G. P. Alexander, S. Ramaswamy, and A. Maitra, *Phys. Rev. Lett.* **126**, 248001 (2021).
- [72] S. Fürthauer, M. Stempel, S. W. Grill, and F. Jülicher, *Phys. Rev. Lett.* **110**, 048103 (2013).
- [73] R. Zhang, A. Mozaffari, and J. J. de Pablo, *Sci. Adv.* **8**, eabg9060 (2022).
- [74] P. W. Ellis, D. J. Pearce, Y.-W. Chang, G. Goldsztein, L. Giomi, and A. Fernandez-Nieves, *Nat. Phys.* **14**, 85 (2018).
- [75] L. Metselaar, J. M. Yeomans, and A. Doostmohammadi, *Phys. Rev. Lett.* **123**, 208001 (2019).
- [76] D. J. G. Pearce, P. W. Ellis, A. Fernandez-Nieves, and L. Giomi, *Phys. Rev. Lett.* **122**, 168002 (2019).
- [77] M. Clairand, A. Mozaffari, J. Hardoüin, R. Zhang, C. Doré, J. Ignés-Mullol, F. Sagués, J. J. de Pablo, and T. Lopez-Leon, *arXiv:2303.13312*.